HOKKAIDO UNIVERSITY

Title	Shape-Dependent Kinetics of Halide Vacancy Filling in Organolead Halide Perovskites
Author(s)	Okamoto, Takuya; Shahjahan, Md; Biju, Vasudevanpillai
Citation	Advanced optical materials, 9(19), 2100355 https://doi.org/10.1002/adom.202100355
Issue Date	2021-10-04
Doc URL	https://hdl.handle.net/2115/86949
Rights	This is the peer reviewed version of the following article: [Okamoto, T., Shahjahan, Md., Biju, V., Shape-Dependent Kinetics of Halide Vacancy Filling in Organolead Halide Perovskites. Adv. Optical Mater. 2021, 9, 2100355. https://doi.org/10.1002/adom.202100355], which has been published in final form at [https://doi.org/10.1002/adom.202100355]. This article may be used for non-commercial purposes in accordance with Wiley Terms and Conditions for Use of Self-Archived Versions.
Type	journal article
File Information	adom.202100355.pdf

Hokkaido University Collection of Scholarly and Academic Papers : HUSCAP

Shape-dependent Kinetics of Halide Vacancy Filling in Organolead Halide Perovskites

Takuya Okamoto,[a,]* *Md. Shahjahan,*[b] *Vasudevanpillai Biju*[a, b,]*

[a]Research Institute for Electronic Science, Hokkaido University, Sapporo, Hokkaido 001-0020, Japan, [b] Graduate School of Environmental Science, Hokkaido University, Sapporo, Hokkaido 001-0020, Japan.

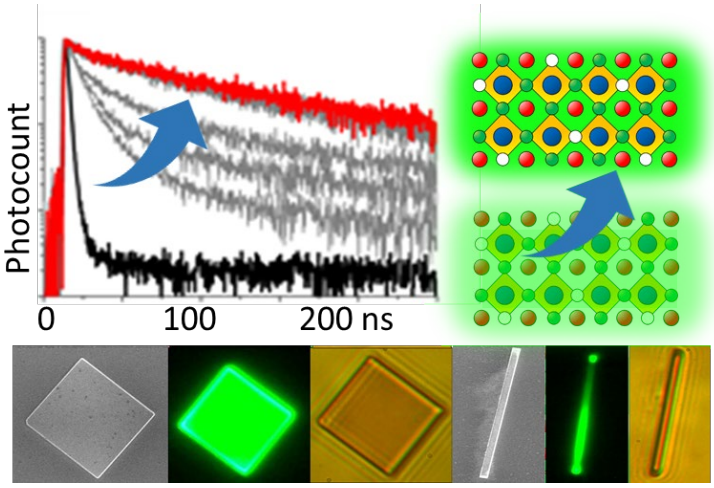
Halide perovskites show high photoluminescence quantum yields and tunable bandgap. While perovskites' optical properties significantly degrade due to the ionic and electronic defects, a correlation among ther structure, size, defects, and degradation rate remains concealed. We report the crystal shape- and halide vacancy-dependent stability of methylammonium lead bromide single crystals. The vacancies are filled in the cubic-, plate-, and rod-shaped crystals by the halide- and light-soaking processes. The differences in the stability, photoluminescence intensity, lifetime, and vacancy filling rates in these geometrical shapes derive from their specific surface-to-volume ratios. The shape-dependent vacancy filling helps us correlate the SEM images, elemental compositions, and the photoluminescence intensity and lifetime.

KEYWORDS

Halide Perovskite, Single Crystals, Crystal Shape, Halide Vacancy, Time-resolved Photoluminescence

∗Email: okamotot@es.hokudai.ac.jp, biju@es.hokudai.ac.jp

Entry for the Table of Contents



Time-resolved light and ion-soaking of $MAPbBr_3$ microcrystals reveals crystal shape- and surface area-dependent halide vacancy filling. The vacancies in a microplate or a microrod are filled within minutes, enormously increasing the photoluminescence intensity and lifetime. The differences in the stability and vacancy filling rates of different crystal geometries are derived from their specific surface-to-volume ratios and nonradiative carrier recombination rates.

Lead halide perovskites (LHPs) are synthesized from simple and cost-effective precursors. These semiconductors show high photoluminescence (PL) quantum yields (QYs), and halide-dependent-tunable bandgap.[1] LHPs have potential applications to lasers, LEDs, and solar cells.[1-3] High-quality LHP single crystals with long-term stability ensure such applications. The ionic and electronic defects significantly reduce the PL QY and durability of an LHP crystal.[4] The carrier lifetime of an LHP crystal depends on these traps, Auger relaxation, and the trap-mediated carrier relaxation, called Shockley–Read–Hall recombination.[5] Thus, defect-free perovskite single crystals for practical optoelectronics are continuously sought after. The defects in an LHP crystal originate from the incomplete formation of the $[BX_6]^-$ octahedra, or the effects of heat, moisture, or oxygen.[6] Although the direct synthesis of a defect-free LHP is challenging, it is essential to classify and reduce defects in various LHP isomorphs.[7]

Halide vacancy filling in LHP nanocrystals, bulk crystals, and thin films improves the sample quality. The oxidation state of the halide vacancies/ions is an important factor in the excitonic and charge carrier properties of perovskites.[4g,h] For example, the hole trap-mediated

nonradiative charge recombination in $CH_3NH_3PbI_3$ is correlated with the oxidation state of the iodine vacancy. [4h] While an I_V^- vacancy does not create a hole trap state, a neutral I_V vacancy forms a hole trap near the conduction band and accelerates nonradiative charge recombination. Similarly, an I_V^+ vacancy accelerates nonradiative charge recombination by forming shallow and deep hole traps. Like I vacancies, Cl or Br vacancies with different oxidation states form shallow and deep traps and influence the nonradiative exciton/charge carrier recombination rate. A chemical additive or photoactivation fills these anion vacancies. In the former case, halide ions from halogen gases,[8] halogen compounds AX[9] (A = MA/FA/Cs/Na/K and X = Cl/Br/I), organic pseudohalides,[10] or ligands[11] fill the vacancies. In the latter case, the so-called light soaking effect, molecules like oxygen improve the PL of LHPs by photoinduced defect passivation.[6c,d,12] For example, superoxide generated by self-sensitization occupies the halide vacancy and improves the optical properties of LHPs.[6c,f] Also, an oxide layer (e.g., PbO) on the LHP surface increases the sample stability against humidity and decreases the trap-assisted nonradiative recombination rate.[6e] Defect passivation during photoexcitation involves lattice expansion and compositional redistribution through ion migration.[12a,b,h] Crystal shapes and optical properties are equally important for the electro-optical applications of LHPs.[3a,13] Information about the LHP crystal shape-dependent halide vacancy filling by a halide precursor or the light can help optimize the properties and applications of LHPs. Nevertheless, a correlation among the structure, shape, size, defects and degradation rate of perovskites remains concealed.

We report the surface-to-volume (s-t-v) ratio-dependent PL stability, halide vacancy filling, -and carrier recombination rates in methylammonium lead bromide ($MAPbBr_3$) single crystals with the cubic, plate, or rod shape. The Br^- vacancies are filled by soaking the crystals in a MABr solution or a picosecond laser beam. We discuss the s-t-v ratio-dependent kinetics

of Br^- vacancy filling from the viewpoint of redistribution in the radiative and nonradiative recombination rates.

Results and Discussion

To investigate the shape-dependent halide vacancy filling, we synthesized $MAPbBr_3$ microrods, microplates, and microcubes. Synthesis procedures and optical and microscopic characterization of the crystals are given below (SI). Figure 1a-c shows the optical microscopic

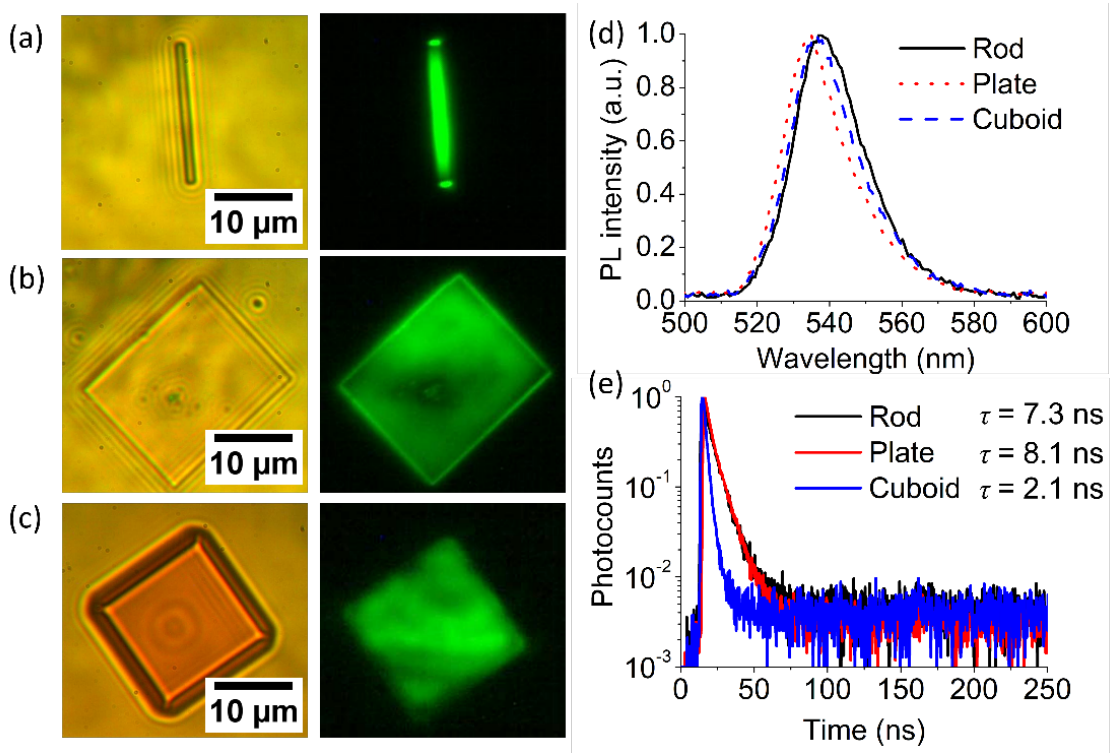


Figure 1. (a-c) Bright-field and PL microscopic images of (a) a microrod, (b) a microplate, and (c) a microcube. (d) PL spectra and (e) PL decay curves of the microcrystals. The PL spectra and PL decays are for the crystals soaked in a solvent mixture (IPA and HDC) but without any MABr.

images, including the PL images, of the three types of crystals.The green PL image, the PL spectra, and decay curves are the characteristics of $MAPbBr_3$ microcrystals. The PL decay curves of the microcrystals fit the third exponential equation (1)

$$y(t) = \alpha_0 + \alpha_1 e^{(-t/\tau 1)} + \alpha_2 e^{(-t/\tau 2)} + \alpha_3 e^{(-t/\tau 3)} \qquad (1)$$

where $\tau n_{(\tau_1/\tau_2/\tau_3)}$ represents the lifetime component and $\alpha_{n\ (\alpha_1/\alpha_2/\alpha_3)}$ the amplitudes. α_0 is a constant. One lifetime component comes from the band-to-band recombination (a radiative relaxation) and the rest to trap-assisted nonradiative recombination.[5a] The average PL lifetimes of the microcrystals were obtained by using the equation (2)

$$\tau_{PL} = \Sigma\alpha_n\tau_n/\Sigma\alpha n \qquad (2)$$

The average PL lifetimes of the $MAPbBr_3$ microrod, microplate, and microcube are 7.3, 8.1, and 2.1 ns, respectively.

To correlate the shapes and s-t-v ratios of LHPs to the halide vacancy-assisted carrier recombination, we investigated the PL lifetimes of the microrod, microplate, and microcube crystals. Figure 2 shows the optical microscope images (insets), PL images (insets), PL decay

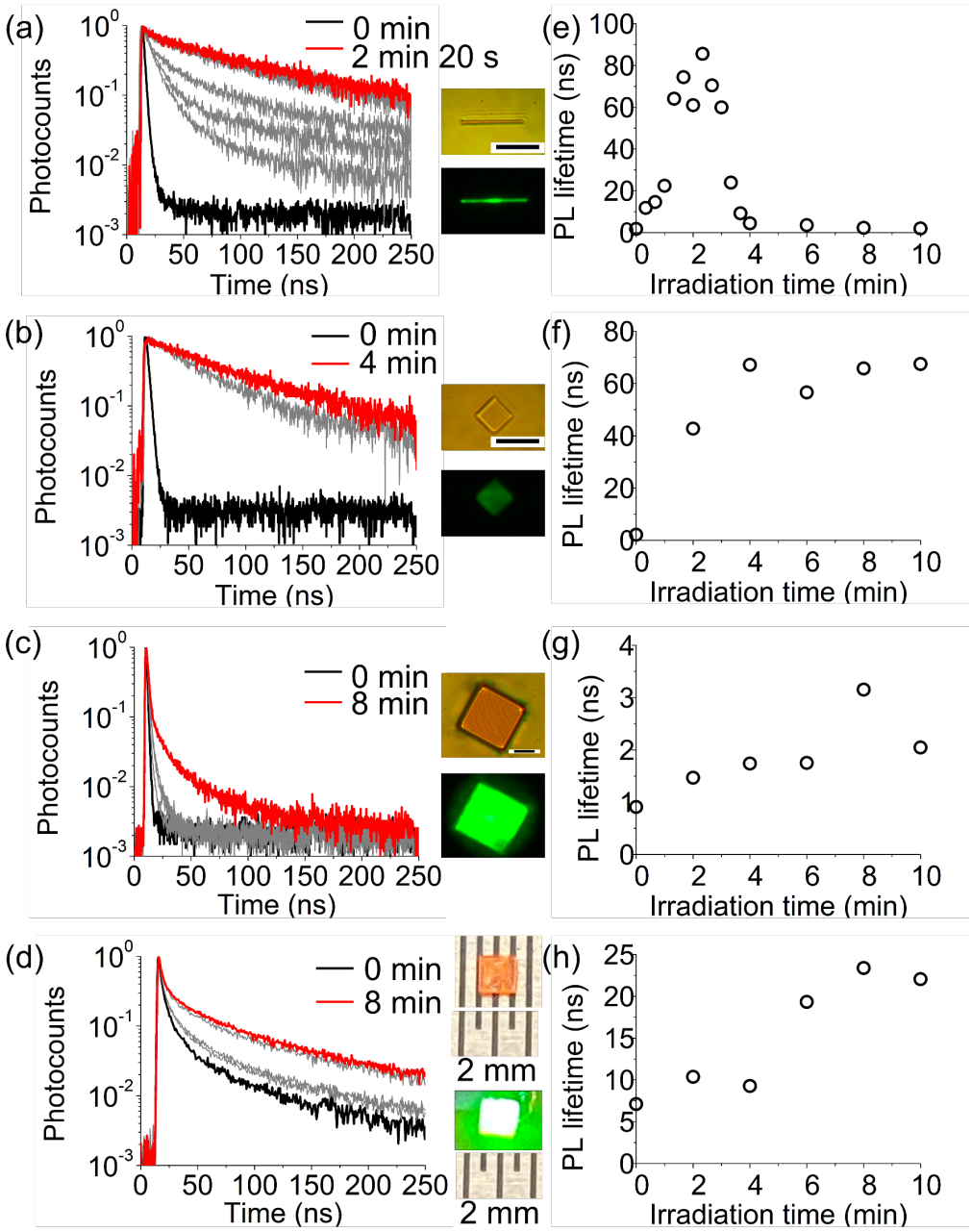


Figure 2. (a-d) the PL decay curves until the PL lifetimes maximizes for (a) a microrod, (b) a microplate, (c) a microcube, and (d) a 1 mm size crystal. Insets: optical microscope and PL images of the microcrystals (scalebar: 10 µm). (d-h) Temporal PL lifetime evolutions for (d) the microrod, (e) the microplate,(f) the microcube, and (h) a 1 mm size crystal.

curves, and PL lifetimes of the crystals. The PL lifetime was enormously increased (from ca 2 to ca 85 ns) for a microrod soaked in a MABr solution within 2 min irradiation with the ps laser (Figure 2b). However, the PL lifetime was decreased by further laser irradiation. Similarly, a microplate's PL lifetime was increased (from ca 2 to ca 67 ns, Figure 2d) within 4 min

irradiation. After 4 min, the PL lifetime became stable. Conversely, the PL lifetime of a microcube soaked in a MABr solution was increased only slightly (from ca 900 ps to ca 3.2 ns) by the irradiation for 10 min or longer (Figure 2f). Several microcrystals of each shape (Figure S1, Supporting Information) showed such changes to the PL lifetime. The 35- to 45-fold lifetime increases for microrods and microplates are related to enormous PL intensity increases. We attribute these increases to photoinduced Br^- vacancy filling. Such an increase was also observed for large crystals. For example, the PL decays and lifetimes of a MAPbBr3 crystal with a 1 mm edge length are shown in Figure 2 (d, h).

After an initial increase, the PL lifetime values decreased by the further ps laser irradiation, which indicates the initial curing and the subsequential activation of Br^- vacancies. The constant PL lifetimes of microplates under prolonged laser irradiation in a MABr solution indicate the stable equilibrium between the Br^- vacancy quenching and activation. Despite the PL lifetime changes, the MABr- or light-soaked microcrystals maintained their shapes. The PL lifetimes of a $MAPbBr_3$ microcrystal before and after the MABr treatment are given by

$$\tau_0 = \frac{1}{k_r + k_{nr} + k_{nr\mathrm{Br}_V}} \tag{3}$$

$$\tau_1 = \frac{1}{k_r + k_{nr}} \tag{4}$$

where τ_0 is the PL lifetime of a $MAPbBr_3$ microcrystal before MABr treatment. τ_1 is the PL lifetime maximum after the treatment, k_r the radiative rate, k_{nr} the nonradiative rate through defects other than the Br^- vacancies, and k_{nrBrV} is the Br^- vacancy-assisted nonradiative rate. The values of τ_1 are higher than τ_0 in all the crystal types due to Br^- vacancy filling. For the crystals in Figure 2, we estimated $k_{nr\mathrm{Br}_V}$ at 5.4×10^8 (microrod), 4.4×10^8 (microplate), and 8.0×10^8 s^{-1} (microcube). As shown in Figure S3, other microcrystals follow a similar trend. Although there is a difference in the k_{nrBrV} values, the rates are comparable in their order of

magnitude. The order of k_{nrBrV} indicates the number of passivated Br^- vacancies until the PL lifetime reaches the maximum value.

We recorded the crystals' PL and SEM images to verify the crystal geometry after MABr- and light-soaking. Figure 3 shows the optical, PL, and SEM images of a microrod, a microplate,

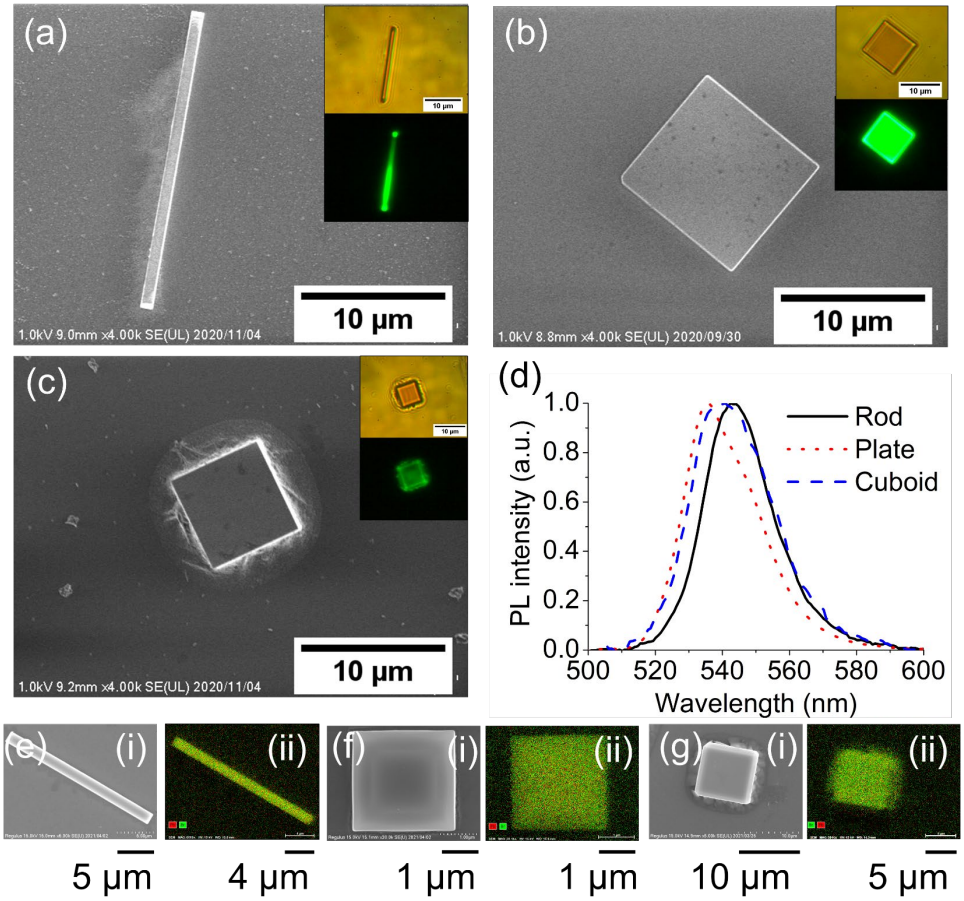


Figure 3. SEM images and PL spectra of (a) a microrod, (b) a microplate, and (c) a microcube after ps laser irradiation in the MABr solution. Insets: brightfield and PL images. (d) The PL spectra of the microcrystals. (e-g) (i) SEM images and (ii) EDX elemental maps (Br: green and Pb: red) of (e) a microrod, (f) a microplate, and (g) a microcube.

and a microcube. These images are for the crystals after the laser irradiation in a MABr solution, showing that the crystals maintain the cubic crystalline phase after the MABr and laser treatments. The shape-depend changes to PL lifetimes (Figure S2) of these crystals are similar to the results shown in Figure 2. Table 1 shows the correlation among the shape, the s-t-v ratios, and the PL lifetime values of the three types of crystals. We estimated the s-t-v ratios from the lateral dimensions and heights of the crystals in the horizontal and tilted SEM images (Figure

S4). Interestingly, the enormous increases in the PL lifetimes of the microplates and microrods indicate that the rate of vacancy filling is higher for the crystals with the large s-t-v ratios. We also verified the Br^- vacancy filling by MABr using SEM-EDX measurement for these three geometries [Figure 3 (e-g)]. We observed a 2 to 5 % increase in the Br component, indicating the percentage of Br vacancy and vacancy filling. Also, the Br content was decreased in some crystals, attributed to the electron beam-induced crystal damage.

Table 1. Surface areas, volumes, and the s-t-v ratios of $MAPbBr_3$ microcrystals, estimated from the SEM images and the PL lifetimes.

	Area (μm^2)	Volume (μm^3)	S-T-V ratio (μm^{-1})	PL lifetime (ns)
Microplate	202.5	23.9	8.5	ca 6 to 138
Microrod	112.7	32.0	3.5	ca 7 to 27
Microcube	183.8	131.4	1.4	ca 1 to 8

Finally, we discuss the shape-dependent defect filling kinetics in LHP microcrystals with the halide vacancy filling mechanism (Figure 4).[14] Low PL intensities and short PL lifetimes of the initial $MAPbBr_3$ microcrystals suggest nonradiative exciton/carrier recombination through the Br^- vacancies. Thus, the PL lifetime and intensity were increased

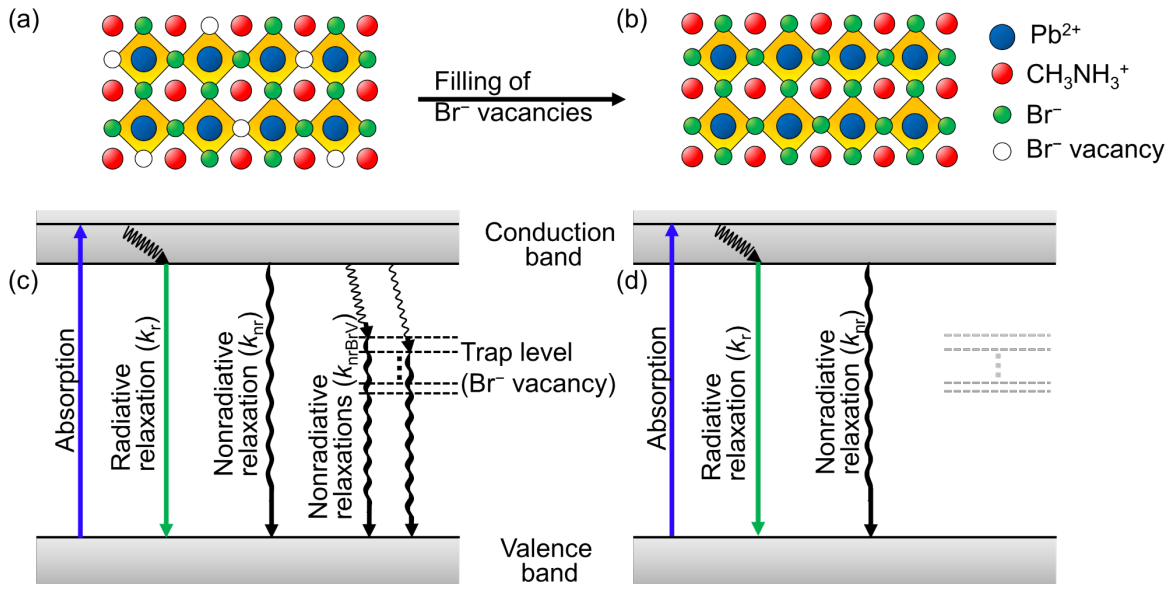


Figure 4. The mechanisms of (a,b) vacancy filling in a $MAPbBr_3$ crystal, and (c,d) the corresponding carrier recombination pathways.

by suppressing the k_{nrBrV} component. As the s-t-v ratio of the $MAPbBr_3$ microcrystals increases, the rate at the PL lifetime increases also becomes higher. The differences in the rate of change of PL lifetime are related to the vacancy filling mechanism. There are two routes of this filling: the spontaneous filling and the light-soaking effect. The light-independent vacancy filling is operative only on the surface of a microcrystal. The surface and grain boundaries are passivated mainly by this method.[9c]

In the light-dependent vacancy filling mechanism, photoinduced ion migration[12] plays a crucial role by accelerating the collision frequency between the positive-charged vacancies in a crystal and Br^- ions in a MABr solution. However, most of the excitation photons are absorbed by a crystal surface. The photon infiltration exponentially decreases within a few hundred nanometers from a crystal surface,[12c] which controls photoinduced ion migration in an LHP crystal.[12d] Therefore, rates at PL lifetimes increase, and the vacancy filling depends on the s-t-v ratios of an LHP crystal.

In summary, we report the shape- and surface-to-volume ratio-dependent halide vacancy filling kinetics of LHP microcrystals. MABr- and light-soaking increase the PL lifetime values of $MAPbBr_3$ microrods, microplates, and microcubes. The 35- to 45-fold increases in the PL lifetimes of the microrods and microplates associate with enormous PL intensities. Increases in PL intensities and lifetimes are due to Br^- vacancy filling. The differences in the photoinduced Br^- vacancy filling are derived from the shape and the specific surface area of single crystals. The shape- and surface-to-volume ratio-dependent halide vacancy filling should be useful for shape-dependent applications of LHPs.[3a,13] The pre-treatment of perovskite with the Br^- vacancy filling should suppress undesired nonradiative recombination in practical photonic device application (e.g. LED, solar cell and photodetector).

Experimental Methods.

Materials: We used the following chemicals without further purification: CH_3NH_3Br (MABr) (TCL, >98.0%), $PbBr_2$ (Aldrich, ≥98.0%), DMF (Wako, ≥99.5%), *N*-cyclohexyl-2-pyrrolidone (CHP) (Aldrich, 99.0%), γ-butyrolactone (GBL) (TCL, >99.0%), isopropyl alcohol (IPA) (≥99.9%) and 1-hexadecene (HDC) (TCL, >90.0%).

***Preparation of $MAPbBr_3$ microcrystals*:** We synthesized the three microcrystals using a literature method with minor modification.[1] A precursor solution of $MAPbBr_3$ in DMF was prepared. In the case of the microcubes synthesis, CHP was added to the 0.05 M $MAPbBr_3$ precursor solution (5 vol %). 10 μL each of this was placed on 25×25 mm^2 cover glasses equipped a silicone rubber O-rings well (sample chamber). The slides were heated (80 °C) for 30 min. For microrod and the microplate synthesis, the $MAPbBr_3$ precursor solution (1M) was prepared in a mixture of DMF and GBL (1:1). 15 μL of this solution was dropped on the sample chamber. The crystallization of the microrods and the microplates was carried out at room temperature. We added 200 μL of the $MAPbBr_3$ precursor solution (1M) to a $MAPbBr_3$ crystal with a 1 mm edge length. The crystallization of the crystals was carried out at 80 ℃ for 20 min. The 1 mm size $MAPbBr_3$ crystal was transferred from the reaction bottle to the sample chamber for further analysis of its PL properties.

***PL decay recording*:** For PL decay measurements, we used a fluorescence microscope, and the sample was excited with a picosecond (ps) laser (Advanced Laser Systems, 465 nm, 45 ps, 1 MHz). PL decays were collected with a TCSPC assembly composed of an APD (Perkin Elmer, SPCM-AQRH) and a TCSPC module (Becker & Hickl GmbH, SPC-830). The ps laser intensity was decreased during PL decay measurements by using an ND filter. The field of detection was restricted by an iris placed in front of the photodetector to collect PL from a selected crystal. The lifetime of microcrystals in the IPA: HDC mixture was measured without any MABr.

***Photo-induced Br^- vacancy filling*:** A saturated MABr solution in 1:9 (v:v) IPA and HDC mixture was prepared for Br^- vacancy filling. After adding a MABr solution into the sample chamber, the sample was exposed to the ps laser (465 nm, 45 ps, 35 pJ 1 MHz). The time evolutions of the PL lifetime of $MAPbBr_3$ microcrystals were traced under air at room temperature.

***Characterization of $MAPbBr_3$ microcrystals*:** The size and morphology of $MAPbBr_3$ microcrystals were analyzed by an optical microscope (OLYMPAS, IX71) and a scanning electron microscope (SEM) (HITACHI, SU8230). The optical transmittance and PL images and PL spectra of $MAPbBr_3$ microcrystals were measured by a CCD camera plus a spectrometer (Ocean Optics, QE65 Pro), respectively. SEM was operated at an acceleration voltage of 1 kV. For the preparation of specimens for SEM observations, the silicone rubber O-rings well was removed from the sample chamber after photoinduced filling of the Br^- vacancy. The $MAPbBr_3$ microcrystals were dried under reduced pressure for 2 hours and then placed in a desiccator for 1 day. For SEM-EDX measurements, the microcrystals were prepared on ITO glass plates. The elemental mapping analysis of a microcube, a microplate, and a microrod before and after the Br^- vacancy filling was carried out using a Bruker SEM-EDX (QUANTAX EDS) operated at 15 kV).

ASSOCIATED CONTENT

Supporting Information.

The Supporting Information (Figures S1 – S4) is available free of charge at www.wiley.comxxx at DOI:

Author Contributions

V. B. conceived the project. T. O. synthesized and characterized the microcrystals. V. B., M. S. and T. O. recorded the PL properties of the crystals. T. O. and V. B. wrote the manuscript.

Funding Sources

This research was supported by the JSPS KAKENHI Grant Number 20J00974, 21K14580 and 19H02550. We acknowledge the Hokkaido University Nanotechnology PLATFORM, the JSPS Dynamic Alliance for Open Innovation Bridging Human, Environment, and Materials, and the Photoexcitonix Program.

The authors declare that they have no conflict of interest

REFERENCES

[1] a) A. Kojima, K. Teshima, Y. Shirai, T. Miyasaka, *J. Am. Chem. Soc.* **2009**, *131*, 6050-6051; b) S. D. Stranks, H. J. Snaith, *Nat. Nanotechnol.* **2015**, *10*, 391-402; c) L. Chouhan, S. Ghimire, C. Subrahmanyam, T. Miyasaka, V. Biju, *Chem. Soc. Rev.* **2020**, *49*, 2869-2885.

[2] Z. K. Tan, R. S. Moghaddam, M. L. Lai, P. Docampo, R. Higler, F. Deschler, M. Price, A. Sadhanala, L. M. Pazos, D. Credgington, F. Hanusch, T. Bein, H. J. Snaith, R. H. Friend, *Nat. Nanotechnol.* **2014**, *9*, 687-692.

[3] a) W. Zhang, L. Peng, J. Liu, A. Tang, J. S. Hu, J. Yao, Y. S. Zhao, *Adv. Mater.* **2016**, *28*, 4040-4046; b) H. Zhu, Y. Fu, F. Meng, X. Wu, Z. Gong, Q. Ding, M. V. Gustafsson, M. T. Trinh, S. Jin, X. Y. Zhu, *Nat. Mater.* **2015**, *14*, 636-642.

[4] a) H. Uratani, K. Yamashita, *J. Phys. Chem. Lett.* **2017**, *8*, 742-746; b) P. Fassl, Y. Zakharko, L. M. Falk, K. P. Goetz, F. Paulus, A. D. Taylor, J. Zaumseil, Y. Vaynzof, *J. Mater. Chem. C* **2019**, *7*, 5285-5292; c) H. D. Jin, E. Debroye, M. Keshavarz, I. G. Scheblykin, M. B. J. Roeffaers, J. Hofkens, J. A. Steele, *Materials Horizons* **2020**, *7*, 397-410; d) S. G. Motti, D. Meggiolaro, S. Martani, R. Sorrentino, A. J. Barker, F. De Angelis, A. Petrozza, *Adv. Mater.* **2019**, *31*, e1901183; e) T. S. Sherkar, C. Momblona, L. Gil-Escrig, J. Avila, M. Sessolo, H. J. Bolink, L. J. A. Koster, *ACS Energy Lett.* **2017**, *2*, 1214-1222; f) S. Singh, Laxmi, D. Kabra, *J. Phys. D-Appl. Phys.* **2020**, *53*; g) J. He, W.-H. Fang, R. Long, *Chem. Sci.* **2019**, *10,* 10079–10088; h) W. Li, Y.-Y. Sun, L. Li, Z. Zhou, J. Tang, O. V. Prezhdo, *J. Am. Chem. Soc.* **2018**, *140*, 15753–15763.

[5] a) E. Aydin, M. De Bastiani, S. De Wolf, *Adv. Mater.* **2019**, *31*, e1900428; b) M. Maiberg, T. Holscher, S. Zahedi-Azad, R. Scheer, *J. Appl. Phys.* **2015**, *118*.

[6] a) Y. H. Chen, H. P. Zhou, *J. Appl. Phys.* **2020**, *128*; b) T. K. O. Vu, D. U. Lee, K. S. Lee, D. Y. Park, M. S. Jeong, E. K. Kim, *Appl. Phys. Lett.* **2019**, *115*; c) J. He, W.-H. Fang, R. Long, O. V. Prezhdo, *J. Am. Chem. Soc.* **2019**, *141*, 5798–5807; d) J. He, W.-H. Fang, R. Long, O. V. Prezhdo, *J. Am. Chem. Soc.* **2020**, *142,* 14664–14673; e) W. Kim, J. B. Park, H. Kim, K. Kim, J. Park, S. Cho, H. Lee, Y. Pak, G. Y. Jung, *J. Mater. Chem. A* **2019**, *7*, 20832–20839; f) L Chouhan, S Ghimire, V Biju, *Angew. Chem.* **2019**, *131*, 4929–4939.

[7] X. X. Chen, S. J. Cheng, L. Xiao, H. D. Sun, *J. Phys. D-Appl. Phys.* **2020**, *53*, 373001.

[8] D. O. Tiede, M. E. Calvo, J. F. Galisteo-Lopez, H. Miguez, *J. Phys. Chem. C* **2018**, *122*, 27250-27255.

[9] a) L. Zhang, X. Z. Zhang, X. X. Xu, J. Tang, J. H. Wu, Z. Lan, *Energy Technol.* **2017**, *5*, 1887-1894; b) N. Wang, Y. Zhang, P. Zeng, Y. Hu, F. Li, M. Liu, *J. Appl. Phys.* **2020**, *128;* c) M. Abdi-Jalebi, Z. Andaji-Garmaroudi, S. Cacovich, C. Stavrakas, B. Philippe, J. M. Richter, M. Alsari, E. P. Booker, E. M. Hutter, A. J. Pearson, S. Lilliu, T. J. Savenije, H. Rensmo, G. Divitini, C. Ducati, R. H. Friend, S. D. Stranks, *Nature* **2018**, *555*, 497-501; d) C. Bi, X. Zheng, B. Chen, H. Wei, J. Huang, *ACS Energy Lett.* **2017**, *2*, 1400–1406; e) L. Qiao, W. Fang, R. Long, O. V. Prezhdo, *Angew Chem. Int. Ed.* **2020**, 59, 4684–4690; f)

[10] X. P. Zheng, S. Yuan, J. K. Liu, J. Yie, F. L. Yuan, W. S. Shen, K. X. Yao, M. Y. Wei, C. Zhou, K. P. Song, B. B. Zhang, Y. B. Lin, M. N. Hedhili, N. Wehbe, Y. Han, H. T. Sun, Z. H. Lu, T. D. Anthopoulos, O. F. Mohammed, E. H. Sargent, L. S. Liao, O. M. Bakr, *ACS Energy Lett.* **2020**, *5*, 793-798.

[11] a) X. Zheng, Y. Hou, H. T. Sun, O. F. Mohammed, E. H. Sargent, O. M. Bakr, *J Phys Chem Lett* **2019**, *10*, 2629-2640; b) D. Xin, S. Tie, R. Yuan, X. Zheng, J. Zhu, W. H. Zhang, *ACS Appl. Mater. Interfaces* **2019**, *11*, 44233-44240.

[12] a) D. W. deQuilettes, W. Zhang, V. M. Burlakov, D. J. Graham, T. Leijtens, A. Osherov, V. Bulovic, H. J. Snaith, D. S. Ginger, S. D. Stranks, *Nat. Commun.* **2016**, *7*, 11683; b) A. Walsh, S. D. Stranks, *ACS Energy Lett.* **2018**, *3*, 1983-1990; c) D. R. Ceratti, Y. Rakita, L. Cremonesi, R. Tenne, V. Kalchenko, M. Elbaum, D. Oron, M. A. C. Potenza, G. Hodes, D. Cahen, *Adv. Mater.* **2018**, *30*; d) H. Choi, J. C. R. Ke, S. Skalsky, C. A. Castle, K. X. Li, K. L. Moore, W. R. Flavell, P. Parkinson, *J. Mater. Chem. C* **2020**, *8*, 7509-7518; e) H. Tsai, R. Asadpour, J. C. Blancon, C. C. Stoumpos, O. Durand, J. W. Strzalka, B. Chen, R. Verduzco, P. M. Ajayan, S. Tretiak, J. Even, M. A. Alam, M. G. Kanatzidis, W. Nie,

A. D. Mohite, *Science* **2018**, *360*, 67-70; f) J. F. Galisteo-López, M. E. Calvo, H. Míguez, *ACS Appl. Energy Mater.* **2019**, *2*, 6967-6972; g) J. He, Y. Zhu, W. Fang, R. Long, The *J. Phys. Chem. Lett.* **2021**, 12, 1664–1670; h) S. Ghimire, L. Chouhan, Y. Takano, K. Takahashi, T. Nakamura, K. Yuyama, V. Biju, *ACS Energy Lett.* **2019**, *4*, 133–141.

[13] a) G. Ghosh, B. Jana, S. Sain, A. Ghosh, A. Patra, *Phys. Chem. Chem. Phys.* **2019**, *21*, 19318-19326; b) H. W. Yang, Y. Z. Zhou, Y. J. Yang, D. Yi, T. Ye, T. D. Lam, D. Golberg, B. Bao, J. N. Yao, X. Wang, *J. Mater. Chem. C* **2018**, *6*, 11707-11713; c) K. Chen, S. Schunemann, S. Song, H. Tuysuz, *Chem. Soc. Rev.* **2018**, *47*, 7045-7077; d) Z. Zuo, J. Ding, Y. Zhao, S. Du, Y. Li, X. Zhan, H. Cui, *J. Phys. Chem. Lett.* **2017**, *8*, 684-689; e) J. F. Galisteo-Lopez, Y. Li, H. Miguez, *J. Phys. Chem. Lett.* **2016**, *7*, 5227-5234.

[14] a) L. Chouhan, S. Ito, E. M. Thomas, Y. Takano, S. Ghimire, H. Miyasaka, V. Biju, *ACS Nano* **2021**, *15*, 2831–2838; b) M. Shahjahan, K. Yuyama, T. Okamoto, V. Biju, *Appl. Mater. Technol.* **2021**, *6*, 2000934.